



The role of rebound spikes in the maintenance of self-sustained neural spiking activity

Bruno Andre Santos · Rogerio Martins Gomes · Phil Husbands

© The Author(s) 2021

Abstract In general, the mechanisms that maintain the activity of neural systems after a triggering stimulus has been removed are not well understood. Different mechanisms involving at the cellular and network levels have been proposed. In this work, based on analysis of a computational model of a spiking neural network, it is proposed that the spike that occurs after a neuron is inhibited (the rebound spike) can be used to sustain the activity in a recurrent inhibitory neural circuit after the stimulation has been removed. It is shown that, in order to sustain the activity, the neurons participating in the recurrent circuit should fire at low frequencies. It is also shown that the occurrence of a rebound spike depends on a combination of factors including synaptic weights, synaptic conductances and the neuron state. We point out that the model developed here is minimalist and does not aim at empirical accuracy. Its purpose is to raise and discuss theoretical issues that could contribute to the understanding of neural mechanisms underlying self-sustained neural activity.

Keywords Self-sustained neural activity · Rebound spike · Neural dynamics · Spiking neurons

1 Introduction

One of the problems in the field of neural dynamics is to understand the mechanisms that enable self-sustained neural activity after a triggering stimulus has been removed. At the cellular level, voltage-dependent conductance activated by specific neuromodulators is an example of a mechanism that generates different rhythmic bursting patterns of action potentials in the absence of synaptic input [12, 20]. By changing local biophysical properties, a neuron can have two or more bursting patterns (stable states) and switch between them when it receives transient excitatory or inhibitory pulses [38]. A variety of empirical works and computational models that reproduce the phenomenon of multistability at the cellular level have been investigated (e.g., [22, 34, 36, 54, 71, 72]). At the network level, recurrent excitatory closed circuits found at different spatial scales—from local cortical circuits to large neural networks encompassing the thalamus and cortex areas, for instance [69]—is an example of another mechanism capable of generating self-sustained activity.

One of the first descriptions of a recurrent excitatory closed circuit was made by Hebb [23]. The central idea of Hebb's proposal is that repeated stimulation of specific synaptic receptors leads slowly to the formation

B. A. Santos (✉) · R. M. Gomes
Federal Centre of Technological Education of Minas
Gerais, Belo Horizonte, Brazil
e-mail: bsantos@cefetmg.br

P. Husbands (✉)
Centre for Computational Neuroscience and Robotics,
University of Sussex, Falmer, Brighton,
United Kingdom
e-mail: p.husbands@sussex.ac.uk

of cell assemblies which are closed circuits that maintain their activity after the end of the stimulation. A variety of works have investigated self-sustained activity at the network level [8,9,33,52,56,66]. Tomov et al. [66] investigated self-sustained neural dynamics—characterized by cycles of intensive global activity followed by moments low activity—by analyzing an hierarchical modular architecture consisting of five classes of inhibitory and excitatory neurons. They found that the duration of self-sustained activity increases with the number of network modules and strongly depends on the initial conditions—suggesting a transient chaotic regime. In a subsequent work [65], the same authors found that inhibitory synapses play an important role in the preparation, start and breakdown of a new epoch of intensive global activity.

Synaptic dynamics has also been proposed to play a role in self-sustained neural activity [14,15,41,60]. As pointed out by Mongillo and colleagues [43], the persistent neural process might not reside entirely in the spiking activity due to the high metabolic cost of action potentials. They propose that short-term synaptic plasticity (*STSP*)—mediated by increased presynaptic calcium levels—is responsible for maintaining the neural activity without enhanced spiking activity. The removal of calcium from presynaptic terminals is a relatively slow process that works as a memory buffer that, when it is loaded, changes the dynamics of the neural system for a short period. The central idea of this activity-silent mechanism is that *STSP* (mediated by calcium buffers, for instance) changes the connections of the network generating temporal neural circuits [58].

Computational and empirical evidence of self-sustained neural activity mediated by *STSP* has been reported in several studies [6,15,16,67]. Fiebig and Lansner [15] developed a computational model of a spiking neural network capable of performing a word-list learning task. They showed that the network capabilities of encoding and reactivation could be reproduced by using *STSP*, namely a fast-expression form of Hebbian synaptic plasticity. Fujisawa and colleagues [16] examined neural activity recordings from the medial prefrontal cortex of the rat moving through a maze. They found that synaptic connections were dynamically modulated by the task allowing the formation of short-term functional neural networks. Various studies have looked at how sustained activity results from specific synaptic plasticity rules, including spike

timing-dependent plasticity (STDP) [13], input timing-dependent plasticity (ITDP) [35,55], and beyond [59].

In this work, another mechanism that could be exploited by neural systems to sustain its activity after the stimulus offset is introduced. The proposed mechanism exploits the spike generated at the end of a period of synaptic inhibition (the rebound spike) to maintain the spiking activity in a closed inhibitory circuit. A computational model is presented that demonstrates the efficacy and properties of the mechanism.

Details of the methodology to develop the computational model are provided in the following section. The mathematical analysis and the discussion are presented in Sects. 3 and 4, respectively.

2 Methods

Some preliminary considerations about the methodology are presented in Sect. 2.1. The task performed by the network is described in Sect. 2.2. Details of the neural network implementation and the methods are presented in Sects. 2.3 and 2.4, respectively.

2.1 Preliminary considerations

The mechanism proposed in this paper is based on the analysis of a computational model of a minimalist spiking neural network. While the task and the types of neurons are predefined, the parameters of the network (synaptic connections and conductance time constants) are adjusted by a genetic algorithm. After adjusting the parameters, the system is analyzed in order to understand how the neural mechanism developed by the genetic algorithm operates. By following these steps, no prior assumption about the operation of the mechanism is built into the model. The mechanism is evolved by the genetic algorithm and then described during mathematical analysis. This type of methodology—without prior assumption built into the model synthesized by the genetic algorithm—allows hypotheses to be raised about neural functioning and has been used by other works in computational neuroscience [26,42,53,68].

It is important to mention that the goal here is not to develop a model with empirical accuracy but to build a minimal model from which theoretical issues about self-sustained neural activity can be raised and dis-

cussed. Minimal models have been used to propose testable hypotheses about the operation of neural systems. Izquierdo and Lockery [30], for instance, proposed a novel neural mechanism for spatial orientation in *Caenorhabditis elegans* based on the analysis of a minimal model consisting of two sensory and two motor neurons. This and other models [5,42,53] reproduce at a merely conceptual level of abstraction a type of dynamics that can be exploited by neural systems to carry out a functional task. They contribute to the understanding of the real neural systems by raising hypothesis and discussing dynamical principles that can be empirically investigated. In the current work, a theoretical, minimal model is also developed aiming at raising a hypothesis that could guide the study of the neural dynamics that outlasts the stimulus.

2.2 Task

The task was designed to be sufficiently rich to require a non-trivial neural mechanism and to be analytically tractable and easily understood. It is inspired by an experiment that consists of presenting a sequence of stimuli to a subject who tries to reproduce it, in the same order, after the presentation of the last stimulus [11,25]. A schematic representation of a trial of the task is presented in Fig. 1. A sequence, among those shown in Table 1, is selected (e.g., S_1). At $t = 25$ ms, the network is stimulated with the first input (e.g., red) and then, at $t = 50$ ms and $t = 75$ ms with the second and the third inputs (e.g., green and blue), respectively. The time interval in which the stimuli is given to the network is referred to as cue period. After a delay period, where no stimulus is applied, the output of the network is analyzed. An output is considered correct if it reproduces the same order of the input sequence (e.g., red, green and blue). The timing between the stimuli does not have to be reproduced, only the order matters.

The task implemented is a simplified version of a memory span test which has been widely used in exper-

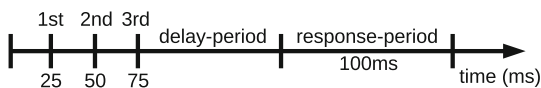


Fig. 1 Trial of the task. Three inputs are presented to the network at $t = 25$ ms, $t = 50$ ms and $t = 75$ ms, respectively. After a time window T (delay period), the output of the network is analyzed for 100 ms (response period)

Table 1 Six different sequences of stimuli that are applied to the network

Sequence	1st	2nd	3rd
S_1	Red	Green	<i>Blue</i>
S_2	Red	<i>Blue</i>	Green
S_3	Green	Red	<i>Blue</i>
S_4	Green	<i>Blue</i>	Red
S_5	<i>Blue</i>	Red	Green
S_6	<i>Blue</i>	Green	Red

Each sequence consists of three different inputs, which can be interpreted as the colors of an object

iments aiming at exploring neural activity [10,46,47]. Note that the model studied here is not intended as a general model of working memory but as a working example of self-sustaining neural activity in a non-trivial context.

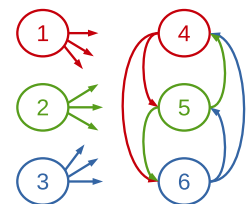
2.3 Network model

A schematic representation of the network is shown in Fig. 2. Neurons 1, 2 and 3 are the input neurons; they do not receive connections from other neurons. Neurons 4, 5 and 6 form a fully connected network and are considered the output of the network. Each output neuron receives connections from all input neurons. In order to stimulate the network, a current is applied to an input neuron so that it fires a spike. The stimulation of each input neuron represents a specific color. Red, blue and green colors are represented by an input current applied to neurons 1, 2 and 3, respectively.

The output neurons 4, 5 and 6 have to reproduce the input sequence presented to neurons 1, 2 and 3, respectively. For example, if the input sequence S_5 (blue, red and green) is applied to the network by stimulating the neurons 3, 1 and 2; then the output neurons 6, 4 and 5 should fire in this order.

Each neuron is implemented by using the Izhikevich spiking neuron model [27,28]. This model has been

Fig. 2 The network has 6 neurons. Three of them receive external stimuli (neurons 1, 2 and 3) and are connected to the other three neurons (4, 5 and 6) which form a fully connected network (Color figure online)



used to study neural dynamics in different contexts [3, 4, 29, 32, 57, 60, 64] and was obtained from simplifications of the Hodgkin–Huxley model [24]. Although it does not reproduce neuronal biological structures, it is capable of simulating several spiking dynamics of real neurons with an efficient computational cost [27, 50]. Izhikevich [28] analyzed a variety of neuron models to identify the number of characteristics of real neurons each model reproduced. He also calculated how many floating-point operations (FLOPS) were required to simulate them. It was shown that the Izhikevich model presents the best balance between computational cost and biological plausibility, which has motivated its use in our work. Despite that, other models capable of generating rebounds could also be used as the mechanism of self-sustained activity introduced here does not require any specific property from the Izhikevich model.

The equations describing the Izhikevich neuron are shown in (1) and (2) with an auxiliary after-spike resetting represented by (3).

$$\frac{dv}{dt} = 0.04v^2 + 5v + 140 - u + I, \quad (1)$$

$$\frac{du}{dt} = a(bv - u), \quad (2)$$

$$\text{if } v \geq 30\text{mV, then } \begin{cases} v \leftarrow c \\ u \leftarrow u + d, \end{cases} \quad (3)$$

where v is the membrane potential of a neuron; u represents the activation of K^+ channels and the inactivation of Na^+ channels, which are responsible for the recovery of the neuron membrane potential. The parameter u provides a negative feedback for v and, after a spike, when v is high ($v \geq 30$), u is incremented by a constant d , as shown in Eq. 3. The parameter I is the input current received from external stimuli or from other neurons (more details are presented throughout this section), a is the decay rate of u , b is the sensitivity of u to subthreshold fluctuations of the membrane potential, c is the reset value of the membrane potential after a spike, and d is the reset value of the variable u after a spike. All neurons used the same fixed set of parameter values ($a = 0.02$, $b = 0.25$, $c = -65$ and $d = 6$). These values were obtained from Izhikevich's prior work and correspond to the Phasic Spiking neuron [28]. By using these parameters, the stable state of the neuron is near the firing threshold, which makes it very sensitive to any stimulation.

The strength of the stimulation (parameter I) applied to the input neurons (1, 2 and 3), at $t = 25$, 50 and 75 ms is equal to 20. The only role of this stimulation is to trigger spikes in the input neurons. With this stimulation, the input neurons fire a spike with a latency of 3 ms, as described in the Results. The input I applied to neurons 4, 5 and 6 is described in Eq. 4.

$$I_i = \sum_j^n W_{ij} g(t)_j, \quad (4)$$

where I_i is the input current for each neuron i and W_{ij} is the synaptic weight from neuron j to neuron i . The function $g(t)_j$ is a postsynaptic conductance model representing the synaptic dynamics. It is calculated by the normalized alpha function [51] described in Eq. 5.

$$g(t)_j = \frac{t}{\tau_j} e^{1 - \frac{t}{\tau_j}}, \quad (5)$$

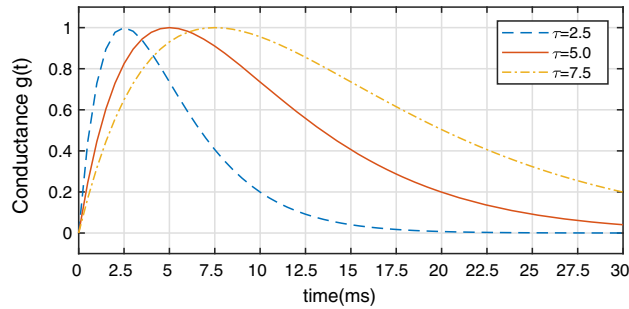
where t is the elapsed time after the spike of the presynaptic neuron and τ_j is the conductance coefficient of neuron j . The behavior of the $g(t)$ for different values of τ is illustrated in Fig. 3.

The value of $g(t)$ varies within $[0, 1]$ and is equal to 1 when $t = \tau$ and equal to 0 when t goes to infinity.

2.4 Parameter optimization

In a successful trial of the experiment, the network should reproduce in its output the same sequence applied to its input neurons. In order to obtain a network capable of performing this task, the microbial genetic algorithm [21] was used to optimize the synaptic weights ($W_{i,j}$) and the time constant τ_i . An initial population of 30 networks was initialized with random values for these parameters. The time constants were initialized within $[0.5, 10]$ and the weights within $[-15, 15]$, allowing inhibitory connections between neurons. In each tournament of the genetic algorithm, the parameters of the losing network (lower fitness) were recombined with the winning network (higher fitness) at a rate of 0.6 and mutated at a rate of 0.05.

The fitness of each network was calculated as follows. An individual of the population is selected and the first sequence S_1 is applied to the input neurons at $t = 25$ ms, $t = 50$ ms and $t = 75$ ms, as represented in Fig. 1. After a time window T of 25 ms, the

Fig. 3 Conductance for different values of τ 

output of the network is analyzed during one hundred milliseconds. If the output neurons reproduce the input sequence, the fitness is incremented by 1. The same steps are repeated for sequences S_2 , S_3 , S_4 , S_5 and S_6 . The maximum fitness of a network should be 6 when it reproduces all input sequences.

Five networks were evolved, each one capable of reproducing the input sequences for a specific delay period ($T = 25, 500, 1000, 1500, 2000$ ms). The analyses of the networks evolved for $T = 25$ ms and $T = 500$ ms will be presented. The operation of the other networks ($T = 1000, 1500, 2000$ ms) is similar to the one evolved for $T = 500$ ms. The networks evolved for $T = 25$ ms and $T = 500$ ms will be referred to as Net_A and Net_B , respectively.

The synaptic conductances τ for Net_A and Net_B are shown in Table 2. The connection weights $W_{i,j}$ for Net_A are shown in Table 3 and for Net_B in Table 4. All these parameters were evolved by the genetic algorithm.

3 Results

An introduction to the role played by the postsynaptic rebound spike in the maintenance of working memory is presented in Sect. 3.1. A more detailed study of this memory mechanism is described in Sect. 3.2.

3.1 Neural network dynamics

The operation of Net_A can be briefly described as follows. During the cue period, when the input sequence is presented, the input neurons fire action potentials. These action potentials hyperpolarize the output neurons due to inhibitory connections from the input neurons to the output ones. During the delay period, the

membrane potentials of the output neurons recover from the inhibition. At the end of the recovery dynamics, in the response period, the output neurons fire rebound spikes in response to the inhibitory synapses. The rebound spikes reproduce the input sequence presented to the network.

Figure 4 shows the spiking dynamics of Net_A . The network correctly reproduced the order of the input sequences in all cases. The inputs neurons are stimulated at 25, 50 and 75 ms and fire action potentials 3 ms later, at 28, 53 and 78 ms, respectively. Notice that, during the cue and delay periods, the information about the input sequence is maintained by the network without firing spikes in the output neurons. The first spike in an output neuron happens at 108 ms for S_6 and at $t = 117$ ms for S_3 . For all sequences (S_1, S_2, S_3, S_4, S_5 and S_6), when the first output neuron spikes, the current generated by the spikes in the input neurons has already ceased.

As described in Eq. 4, the input current of a postsynaptic neuron depends on the time constant τ (Table 2) and on the connection weights $W_{i,j}$ (Table 3). Observe that the connection weights from the input neurons to the output ones are all negative—see the first three columns of Table 3. Figure 5 shows an example of how the input currents of neurons 4, 5 and 6 change over time considering the input sequence S_6 . The input current is $\approx -1 \times 10^{-3}$ at $t = 91$ ms and $\approx -1 \times 10^{-6}$ at $t = 100$ ms. At the moment of the first spike of neuron 6 (at $t = 108$ ms), all input currents are null.

Without input current, the dynamics of the neurons tend to converge to their resting state. However, when the current generated by the inhibitory input neurons (1, 2 and 3) goes to zero, the output neurons are left in a state from which they will fire spikes (the rebound spikes). The state of each neuron when their inputs are near zero is shown in Fig. 6. In Graphic B, neurons 4 (red) and 6 (blue) have already crossed the threshold

Table 2 Time constants (ms) for the synaptic conductance for Net_A and Net_B

Network	τ_1	τ_2	τ_3	τ_4	τ_5	τ_6
Net_A	1.01	2.30	2.30	5.24	9.41	9.44
Net_B	5.90	8.83	7.93	8.23	6.56	7.24

Table 3 Connection weights between neurons for Net_A

i	$W_{i,1}$	$W_{i,2}$	$W_{i,3}$	$W_{i,4}$	$W_{i,5}$	$W_{i,6}$
4	-5.16	-11.39	-10.84	0.00	-10.12	-10.26
5	-6.83	-2.10	-14.14	5.81	0.00	-10.26
6	-14.08	-13.22	-4.00	-2.54	-12.77	0.00

Each line contains the presynaptic weights for a neuron i . The synaptic weight from neuron 1 to 4, for instance, is $W_{4,1} = -5.16$ and from neuron 2 to 4 is $W_{4,2} = -11.39$

Table 4 Connection weights for the network Net_B

i	$W_{i,1}$	$W_{i,2}$	$W_{i,3}$	$W_{i,4}$	$W_{i,5}$	$W_{i,6}$
4	-15.00	-10.56	-4.19	0.00	-15.00	-13.87
5	12.27	0.71	-7.56	-15.00	0.00	4.49
6	-3.72	3.75	5.38	-12.82	-11.84	0.00

Each line contains the presynaptic weights of a neuron i . The weight from neuron 4 to 6, for instance, is $W_{6,4} = -12.82$

Fig. 4 Neural network spikes for each input sequence (see graphic title). Time (ms) is shown in the x-axis and the neuron number (from 1 to 6) in the y-axis. Vertical dashed lines highlight the response period ($t = [100, 200]$ ms) where the output neurons (4, 5 and 6) should reproduce the input sequence

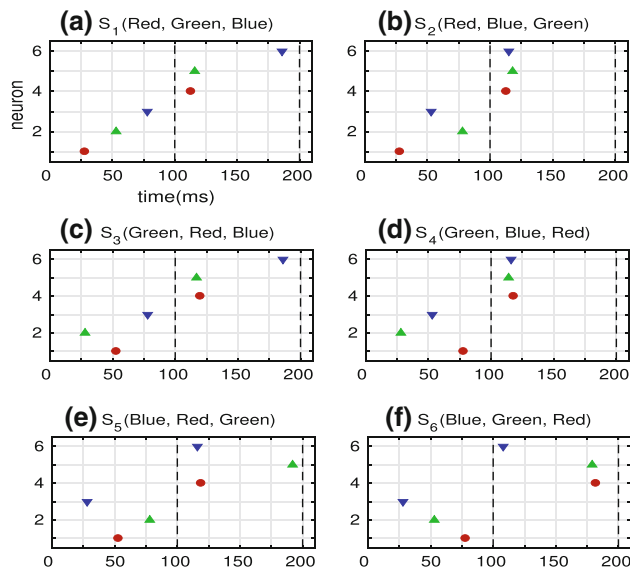
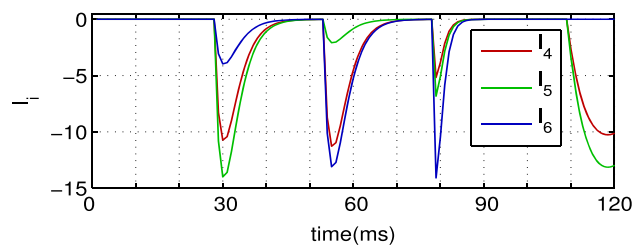


Fig. 5 Input currents (y-axis) for neurons 4, 5 and 6 (see legend) during the presentation of the input sequence S_6 in a time window of 120 ms (see x-axis)



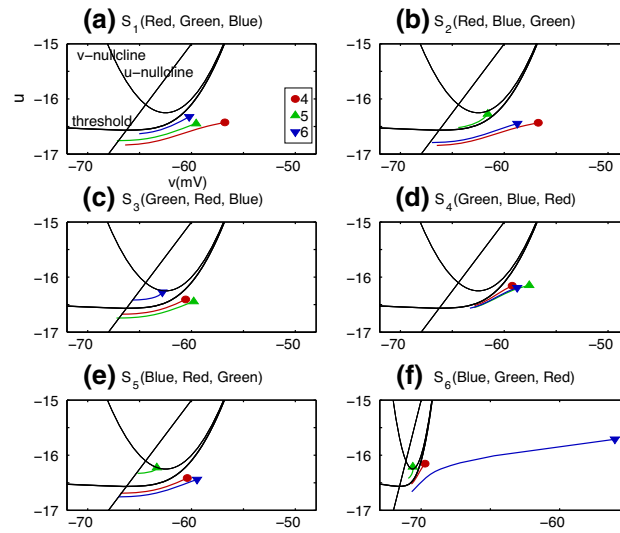


Fig. 6 Trajectories of the output neurons during the time window [91,107] ms for all input sequences (see graphic title). The membrane potential v is shown on the x -axis and the variable u on the y -axis. The dynamics of neurons 4, 5 and 6 are shown by the red, green and blue trajectories, respectively. The state of each neuron at $t = 107$ ms is represented by the colored filled

circle (see legend). Only Graphic F has a different scale for the x -axis. The nullclines for v and u and the firing threshold are identified in Graphic A. The system resting state is given by the point where the nullclines cross each other. The arrows at the top of Graphic A show the direction of the vector field in each region of state space defined by the nullclines (Color figure online)

and will fire. When neuron 4 fires, it excites neuron 5 (green) making it cross the threshold. In Graphic D, all output neurons have already crossed the firing threshold and will fire in the order 5, 6 and 4 (corresponding to green, blue and red colors). In Graphic F, neuron 6 (blue) fires first. Although neuron 4 has already crossed the threshold, it is inhibited by neuron 6 (blue) and fires only after neuron 5 (green).

Summarizing, in Net_A the input neurons inhibit the output neurons during the cue period. At the end of the inhibition, the output neurons fire rebound spikes according to the input sequence presented. The order of the rebound spikes depends on the trajectories of the output neurons in the state space given by v and u . Note that, during the delay period, the information about the input sequence is stored by the output neuron dynamics, *i.e.*, the information is maintained by mechanisms at the cellular level represented in the model by the variables v and u .

Network Net_B differs from Net_A as it requires a network mechanism to maintain the information for a longer period ($T=500$ ms). The firing dynamics of Net_B is shown in Fig. 7. The network correctly repro-

duced the order of the input sequences for all cases. For S_1 (Fig. 7A), for example, neurons 4 (red), 5 (green) and 6 (blue) fire at 587 ms, 663 ms and 664 ms, respectively. While in Net_A the output neurons fire only during the response period, in Net_B they fire after the application of the first input signal (e.g., neuron 5 fires at $t = 32$ ms for S_1 and S_2).

During the delay period, the action potentials of the output neurons are responsible for maintaining the information about the input sequence and do not necessarily reproduce the correct sequence. In Fig. 7D, for instance, the output neurons fire in the order 4 (red) 6 (blue) 5 (green) before generating the correct sequence 5 (green), 6 (blue) and 4 (red) from $t = 575$ ms onwards. (Hence, the output sequence is correct during the response period.) In order to understand how the network activity is maintained during the delay period, the input currents of neurons 4, 5 and 6 were analyzed.

The total input currents for neurons 4, 5 and 6 during the time window [100, 400] ms for S_6 are shown in Fig. 8. Neuron 5 is inhibited during the interval [130, 180] ms (see the negative value of the input current - green

Fig. 7 Neural network spikes for each input sequence (see graphic title). The time (ms) is shown in the x -axis and the neuron identification (from 1 to 6) in the y -axis. Vertical dashed lines highlight the response period ($t = [575, 675]$ ms) where the output neurons (4, 5 and 6) should reproduce the input sequence (Color figure online)

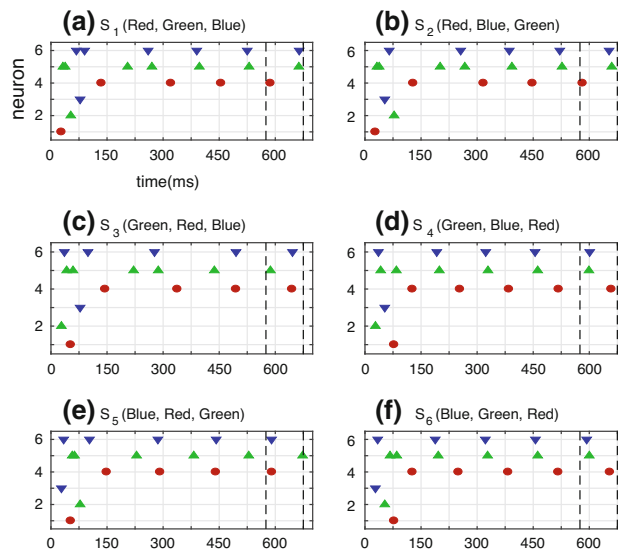
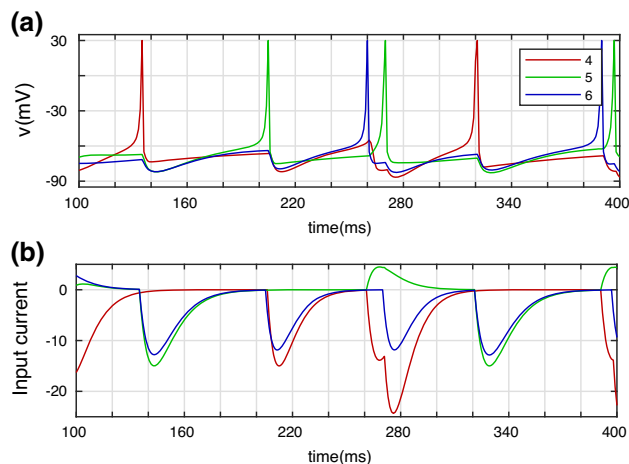


Fig. 8 Membrane potential (Graphic A) and input currents (Graphic B) for neurons 4, 5 and 6 (see legend) at the time window [100, 400] ms (see x -axis) considering trial S_6



line). In the interval $t = [180, 205]$ ms, the input currents tend to zero (at $t = 204$ ms, $I_4 = -0.00001$, $I_5 = -0.078$ and $I_6 = -0.060$) and the neurons approach their resting state (not shown in the graphics). However, at $t = 205$ ms, neuron 5 fires a rebound spike which maintains the activity of the network. Note that, neuron 6 (blue line) is also inhibited during the interval [130, 180] ms but does not fire a rebound spike as it is inhibited again by the spike of neuron 5 at $t = 205$ ms. The inhibition received by neuron 6 at $t = 205$ ms generates a rebound spike at $t = 260$ ms. Note as well that the rebound spikes are responsible for sustaining the network activity, which otherwise would disappear.

A common mechanism in both networks (Net_A and Net_B) is that at the end of a period of synaptic inhibition (when the input current goes to zero), the postsynaptic neuron fires an action potential. While in Net_A the action potentials of the output neurons reproduce the corresponding input sequences, in Net_B they maintain the network activity up to the moment where the input sequence has to be reproduced. This result suggests that in a recurrent spiking neural network, synaptic inhibition followed by a postsynaptic action potential can be used to sustain neural activity after the stimulation has been removed. A more detailed study of this mechanism is presented in the next section.

3.2 Inhibitory synapse and postsynaptic action potential

We now analyze the dynamics and the parameters of the system in order to understand the conditions under which a rebound spike occurs.

3.2.1 Dynamical description

First of all, let us highlight the inhibitory synapses received by the output neurons in both networks (shown in Tables 3 and 4). In Net_A , all synapses are negative except the one from neuron 4 to 5 ($W_{5,4}$). The inhibitory current received by the output neurons during a trial of the experiment is illustrated in Fig. 5. In Net_B , all connections among the output neurons are negative except the one from neuron 6 to 5 ($W_{5,6}$). The input current dynamics is illustrated in Fig. 8B. Despite having one excitatory synapse among the output neurons in each network, our focus is to understand how the inhibitory synapses participate in the maintenance of the neural activity.

Two trajectories of a neuron in the state space, starting from the same initial conditions and different presynaptic weights ($W = -15$ and $W = -9$), were analyzed to understand the neural dynamics at the end of a period of synaptic inhibition. For both trajectories the neuron was initialized at $v = -67.74$ and $u = -15.24$ with presynaptic conductance $\tau = 7.5$. The values of W , v , u and τ were chosen in order to illustrate two types of trajectories, one that converges to the stable point and another that generates a rebound spike. A detailed study of the parameter space is shown in Sect. 3.2.2. Snapshots of the trajectories were taken at 4 different moments: $t = 40$ ms, $t = 50$ ms, $t = 60$ ms and $t = 150$ ms. The snapshots of the trajectory for $W = -15$ are shown in Fig. 9A1–A4 and for $W = -9$ in Fig. 9B1–B4.

As the value of I decreases, the v -nullcline moves upwards (see how the vertex of the parabola changes in Graphics A1, A2, A3 and A4). At $t = 40$ ms and for $W = -15$ (Graphics A1), the system is close to crossing the v -nullcline. Notice that above v -nullcline (see regions R1 and R3) the neuron membrane potential decreases and, if the input current does not change, it will eventually converge to its resting state (the point where the nullclines cross each other). Ten milliseconds later (at $t = 50$ ms, see Graphics A2), the input current is smaller (which moves the v -nullcline upwards),

and the neuron state is very close to crossing the firing threshold (red curve). At $t = 60$ ms (Graphics A3), the neuron membrane potential has already crossed the threshold. At this point, the neuron will fire unless it is inhibited again. At $t = 150$ ms, the input current is near zero 1×10^{-6} and the neuron will fire the rebound spike ($v = 30$ mV, not shown in the graphic).

For $W = -9$ (Graphics B1–B4), as the input decreases the neuron state converges to the resting state. When the neuron state crosses the v -nullcline (see Graphic B4), it moves in the direction of the stable point and does not fire a rebound. Notice that the rebound spike in the postsynaptic neuron happened when the inhibition was stronger ($W = -15$). This result indicates that whether or not a neuron fires at the end of a period of synaptic inhibition depends on the strength of inhibitory connection between the pre- and postsynaptic neurons. The parameter space for W , v , u and τ is studied in the next section.

3.2.2 Influence of the system parameters on the rebound spikes

Whether or not there will be a rebound spike depends on the connection strength (W), on the conductance (τ) and on the state of the postsynaptic neuron (v and u) at the moment the inhibition occurs.

Influence of W and τ on the rebound spike. In order to understand whether or not a combination of W , τ causes a rebound spike, the dynamics of a postsynaptic neuron has been simulated considering: i) presynaptic weights within $W = [-30, -0.5]$; ii) presynaptic conductances within $\tau = [1, 20]$; and five different initial states. The results are shown in Fig. 10.

The closer the neuron is to its resting state (P5), the bigger the set of values of τ and W that will produce rebound spikes. If the inhibition starts from P4 (Fig. 10E), for instance, a spike will happen for most values of $\tau \geq 3$ and $W \leq -8.5$. On the other hand, if the inhibition starts from P1 (Fig. 10B), a spike will happen for a smaller set of values within $\tau \geq 11$ and $W \leq -22$.

The value of τ has a strong influence on the time it takes for the neuron to fire a spike. Notice how the color changes along the x -axis (see the color bar) in Fig. 10B–E. This result was expected because the neuron may fire a rebound only when its input is near zero and, the higher the value of τ , the longer it takes for the input current to go to zero. The synaptic weights also influence the time it takes for the neuron to fire a spike.

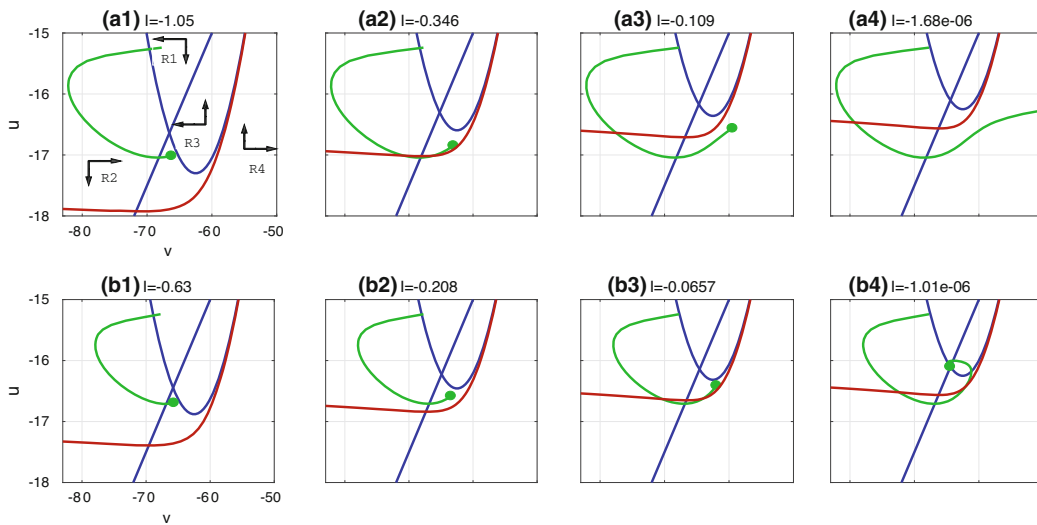


Fig. 9 Dynamics of a neuron under different inhibitory synapses. Graphics A1 (see title) shows the trajectory in the state space (v in the x -axis and u in the y -axis) of a neuron that receives an inhibitory synapse $W = -15$. The initial state of the neuron is $v = -67.74$ and $u = -15.24$. The trajectory (green line) in Graphics A1 depicts the dynamics from $t = 0$ ms to $t = 40$ ms. The state of the neuron at $t = 40$ ms is shown as a green filled circle. The blue parabola represents v -nullcline, and the blue line represents u -nullcline. The red curve shows the firing threshold. After crossing it, a neuron fires a spike unless it is inhibited. The nullclines and the threshold were plotted considering $I = -1.05$, which is the value of the input at $t = 40$ ms

(see graphic title). The arrows represent the direction of the vector field at each region defined by the nullclines. For easier explanation, the regions were identified as R_1 , R_2 , R_3 and R_4 . Graphics A2, A3 and A4 show how the trajectory unfolds in the intervals $[0,50]$ ms, $[0,60]$ ms and $[0,150]$ ms, respectively. The values of I at the end of these intervals are shown in the graphic titles. The nullclines and the threshold in each graphic are different due to different values of I (more details in the text body). The only difference from Graphics B1–B4 is that they show the trajectory for an inhibitory synapse $W = -9$ (rather than $W = -15$). The neuron fires a rebound spike for an inhibition of $W = -15$ and goes to the stable point for $W = -9$ (Color figure online)

Taking P3 as the initial state (Fig. 10D) and $\tau = 15$, the neuron will fire at $t = 109$ ms for $W = -30$ and at $t = 129$ ms for $W = -13.5$. Independently of the initial state, there will not be a rebound spike if $W > -5$ and $\tau \leq -1$ (values taken from Fig. 10F). On the other hand, the neuron will always fire if $W \leq -24.5$ and $\tau \geq 13.5$ (values taken from Fig. 10A).

Influence of v and u on the rebound spike. In order to understand whether or not a combination of v and u causes a rebound spike, the dynamics of a postsynaptic neuron has been simulated considering all possible combinations of v within $[-80, -79.5, -79, -78.5, \dots, -60]$ and u within $[-17, -16.9, -16.8, \dots, -12]$. For each combination, fixed values of W and τ were used (see Fig. 11). Notice that the value of u (on the y -axis) divides the state space into two regions. A rebound spike occurs only in the region below u . In Fig. 11A, for example, rebound spikes occur for values u smaller

than -16.20 . The value of u below which a rebound spike occurs will be referred to as threshold u_{th} .

While the value of u defines a threshold, the value of v (on the x -axis) has a small influence on the occurrence of rebound spikes. For $v = -60$, in Fig. 11A, rebound spikes will occur for all values of $u \leq -16.20$ and for $v = -80$ rebound spikes will occur for $u \leq -16.06$. *Relationship of W , τ and u_{th} .* As the inhibitory synapse W becomes more negative, the threshold u_{th} increases. For example, the thresholds for $W = -5, -10$ and -20 are $u_{th} = -16.08, -14.82$ and -12.7 , respectively (these values are considering $v = -70$, see Fig. 11A–C). On the other hand, as the value of the synapse conductance τ increases, the threshold does not necessarily increase. For example, the thresholds for $\tau = 5, 10$ and 15 are $u_{th} = -15.62, -14.76$ and -17.56 , respectively (these values are considering $v = -70$, see Fig. 11D–F). The relation between the threshold u_{th} and the variables W and τ is shown in Fig. 12.

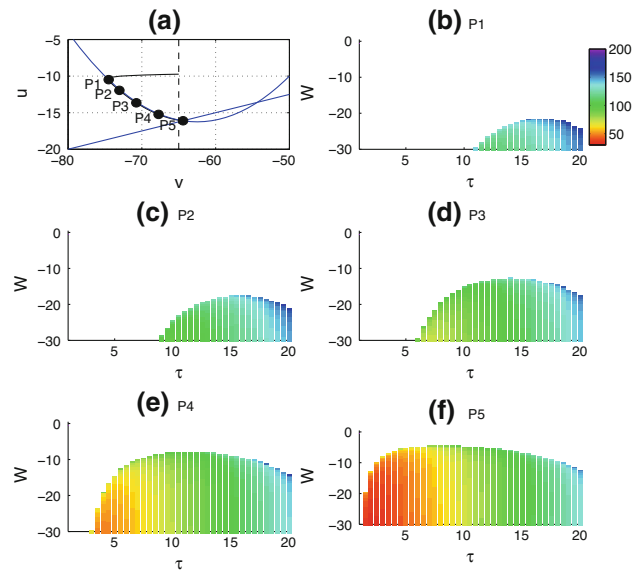


Fig. 10 Effects of the parameters W and τ on the rebound spike of an inhibited neuron. The five different initial states analyzed are represented by the black filled circles in Graphics A. Point P_5 corresponds to the stable state of the neuron. The vertical dashed line, in Graphic A, depicts the after-spike resetting value for v . The blue parabola represents the v -nullcline, and the blue line represents the u -nullcline. Graphics B, C, D, E and F show the

conductance τ on the x -axis, the connection weight W on the y -axis and the initial neuron state in the graphic title. A colored point in these graphics represents the time (in milliseconds) it takes for a neuron to fire a rebound spike, considering $t = 0$ ms at the beginning of the inhibition (see color bar). The white area in these graphics represents combinations of τ and W that do not generate rebound spikes (Color figure online)

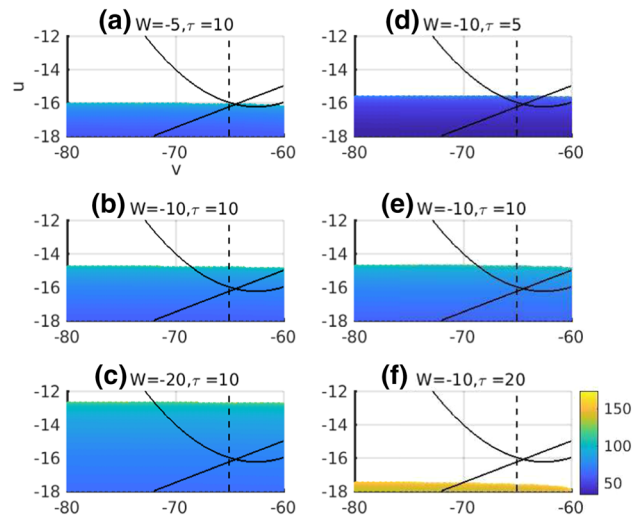


Fig. 11 Effects of the parameters v and u on the rebound spike of an inhibited neuron. The values of W and τ are fixed and shown in the title of each graphic. Vertical dashed lines depict the after-spike resetting value for v . Black parabolas represent v -nullclines, and the black lines represent u -nullclines. The colored

region in these graphics represents the time (in milliseconds) it takes for a neuron to fire a rebound spike considering $t = 0$ ms at the beginning of the inhibition (see color bar). The white region in these graphics represents combinations of v, u that do not generate rebound spikes (Color figure online)

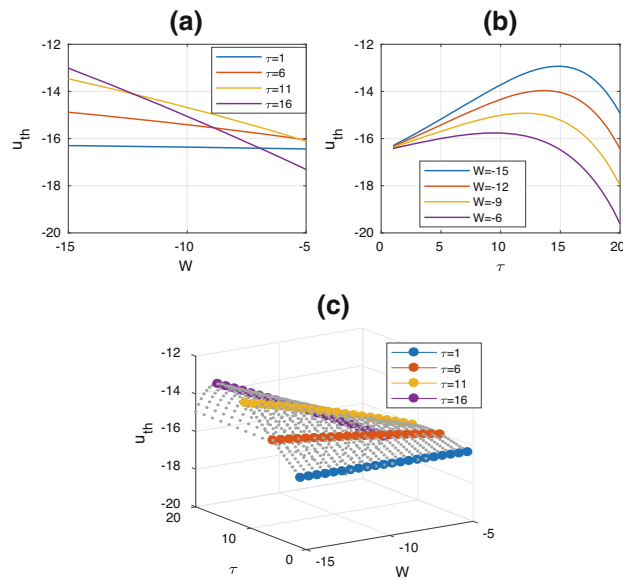


Fig. 12 Relation between the variables W , τ and the threshold u_{th} for a constant $v = 70$. Graphic A shows the synaptic weight W on the x -axis and the threshold u_{th} on the y -axis. The threshold was calculated for four different values of τ (see legend). The rebound spike occurs for values of W and u below the threshold (*i.e.*, below each line). Graphic B shows the synaptic

conductance τ on the x -axis and the threshold u_{th} on the y -axis. The threshold was calculated for four different values of W (see legend). Graphic C shows a threshold surface consisting of W (x -axis), τ (y -axis) and the threshold u_{th} (z -axis). Points below the surface generate a rebound spike (Color figure online)

For an inhibitory synapse $W = -10$ and conductance $\tau = 1$, the postsynaptic neuron fires a rebound spike for values of u below -16.38 (see blue line in Fig. 12A). For a conductance $\tau = 10$ and an inhibitory synapse $W = -15$, the postsynaptic neuron fires a rebound spike for values of u below -13.73 (see blue curve in Fig. 12B). The stronger the inhibition (the more negative), the higher the thresholds and, consequently, more likely is the neuron to fire a rebound spike (see Fig. 12A). Higher values of τ (see x -axis Fig. 12B) increase the threshold up to a certain point and decrease it afterward.

The peak of the surface threshold shown in Graphic C is at $W = -15$ and $\tau = 15$ and the threshold at this point is $u_{th} = -12.95$, which means that when u is above -12.95 , the neuron will not fire a rebound spike for any combination of W and τ . On the other hand, the minimum of the surface threshold is at $W = -5.5$ and $\tau = 19.5$ with a threshold of $u_{th} = -19.51$, which means that when u is below -19.51 , the neuron always fires a rebound spike for any combination of W and τ . For values of u within $[-19.51, -12.95]$, the presence of a rebound spike depends on the values of W

and τ . The surface shown in Fig. 12C summarizes the conditions under which a combination of parameters generates a rebound spike.

When a presynaptic neuron is firing inhibitory spikes at certain frequency, some spikes may occur when the parameter u of the postsynaptic neuron is below u_{th} (causing a rebound spike) and others when u is above u_{th} (not causing a rebound). In this case, the frequencies of these neurons will not necessarily be the same as not all inhibitory spikes will have a corresponding rebound. In the next section, we analyze how the frequency of the inhibitory neuron relates to the frequency of the neuron that generates rebounds.

3.2.3 The relationship between inhibitory and rebound spikes

There are two situations where the inhibitory spike will not have a corresponding rebound. In the first situation, suppose that a presynaptic neuron fires and causes a rebound in the postsynaptic neuron. At the moment the postsynaptic neuron fires, the value of u is increased by a constant d (as described in Eq. 3). This increase

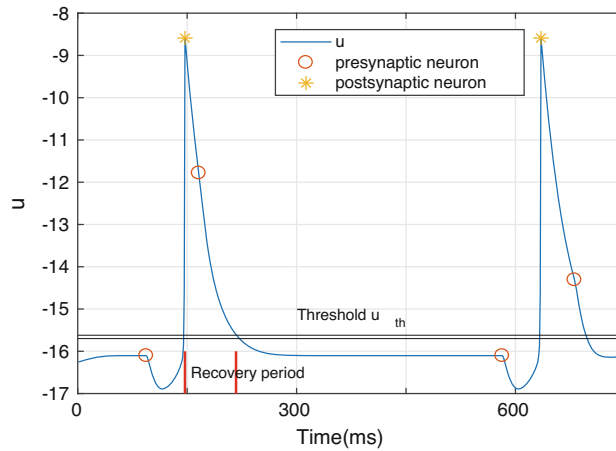


Fig. 13 Recovery period of u . The blue line shows how the parameter u (y -axis) of a postsynaptic neuron changes over time (x -axis). Red circles and yellow asterisks represent a spike in the pre and postsynaptic neurons, respectively (see legend). Horizontal black lines at $u = -15.70$ and $u = -15.62$ highlight the

thresholds u_{th} for $v = -80$ and $v = -60$, respectively. Two vertical red bars highlight the recovery period [147, 217] ms where the value of u is above the thresholds. This simulation was carried out using $W = -10$ and $\tau = 5$ (Color figure online)

pushes the value of u above the threshold. If the presynaptic neuron fires again when u is above the threshold, the inhibition will not cause a rebound spike. The value of u remains above the u_{th} for a short period. During this period, referred to here as the *recovery period* of u , inhibitory synapses will not cause rebound spikes, as illustrated in Fig. 13.

At $t = 94$ ms, the presynaptic neuron spikes and inhibits the postsynaptic neuron. At $t = 147$ ms, the postsynaptic neuron fires a rebound spike. During the next 70 ms ([147, 217] ms), the variable u is above the threshold. During this time window, a spike in the presynaptic neuron will not cause a rebound, which is illustrated by the spike in the presynaptic neuron at $t = 166$ ms followed by the stabilization of u from $t = 300$ ms until $t = 582$ ms when the presynaptic neuron spikes again. Notice that, if the inhibitory presynaptic neuron is firing at a high frequency, some spikes may occur during the recovery period of u and will not have a corresponding rebound.

The second situation is when the presynaptic neuron fires more than once before the postsynaptic neuron has time to fire the rebound. The rebound occurs only at the end of the inhibition processes when the input current I goes to 0, as shown in Figs. 5, 8 and 9. If the presynaptic neuron is firing at high frequencies, some inhibitory spikes may occur before the postsynaptic neuron has time to fire the rebound.

A study on how the frequency of a presynaptic neuron relates to the number of rebound spikes in the postsynaptic neuron is shown in Fig. 14. There will be a one-to-one relationship when the frequency of the presynaptic neuron is less than or equal to 6 Hz, *i.e.*, if the presynaptic neuron fires at frequencies less than or equal to 6 Hz, the postsynaptic neuron will fire rebound spikes at the same frequency. Above 6 Hz, inhibitory spikes start happen during the recovery period of u in the postsynaptic neuron. For 9 Hz, for instance, 50% of the inhibitory spikes take place above the threshold and, consequently, the postsynaptic neuron will fire rebound spikes at 4.5 Hz. For a frequency of 13 Hz, the percentage of spikes in the presynaptic neuron that takes place above u_{th} increases to 53% and the rebound spikes decreases to 47%.

For a frequency of 16 Hz, 33.3% of the inhibitory spikes generate rebounds and the other 66.7% do not generate rebounds. Out of the 66.7%, 60.1% do not generate rebounds as they are above u_{th} and 6.6% are presynaptic spikes that do not wait for the rebound of a previous inhibitory synapse. When the presynaptic neuron fires at frequencies greater than or equal to 23 Hz, the percentage of rebound spikes is zero. The reason is that the postsynaptic neuron is constantly inhibited and does not have time to fire rebound spikes.

In summary, in order to have a one-to-one relationship between the number of inhibitory and rebound

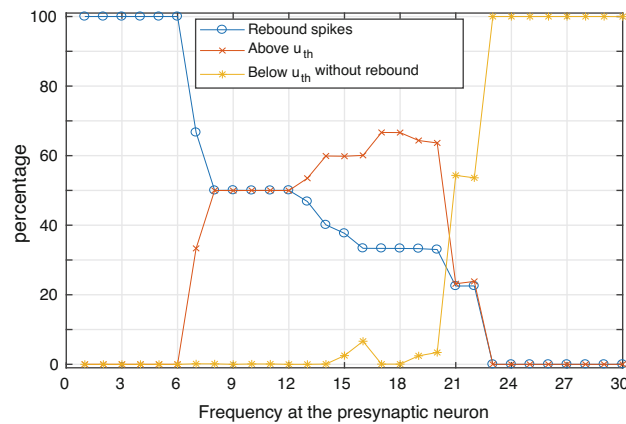


Fig. 14 Relation between inhibitory and rebound spikes. The x -axis shows the frequency of a presynaptic inhibitory neuron. The line with circles (blue line) shows the percentage of rebound spikes generated by the inhibitory spikes of the presynaptic neuron firing at different frequencies (x -axis). Line with crosses (red line) shows the percentage of spikes in the presynaptic neuron that happen above the threshold u_{th} . For example, when the

presynaptic neuron is firing at 12 Hz, 50% of its spikes will happen when the parameter u of the postsynaptic neuron is above u_{th} . Line with asterisks (orange line) shows the percentage of spikes in the presynaptic neuron that occur below the threshold u_{th} and do not cause a rebound spike. This simulation was carried out using $W = -10$ and $\tau = 5$ (Color figure online)

spikes, the presynaptic neuron should fire at low frequencies.

3.3 Dynamics of the system during self-sustained oscillations

To shed further light on the type of behavior (e.g., periodic, quasi-regular, chaotic, etc.) underlying the oscillations sustained by the rebound spikes, we carried out a preliminary analysis of the time series of the neuron membrane potentials (v_3 , v_4 and v_5) for each input sequence (from S_1 to S_6). The method used for the analysis was the 0-1 Test [17–19], which has been previously applied to distinguish chaotic from regular behaviors in Izhikevich spiking neurons [31, 61, 63]. The output of the 0-1 Test is a value K between 0 and 1, with values near 0 indicating regular behavior and values near 1 indicating chaotic behavior. The results from the 0-1 Test are shown in Table 5.

The results of the 0-1 Test suggest that the oscillations sustained by the rebound spikes exhibit chaotic dynamics. However, for all initializing input sequences, the system eventually converges to a stable state. This indicates that the system dynamics might best be thought of in terms of transient chaos [62], which supports previous findings related to self-sustained neural

activity [66]. It is worth noting that the time taken for the oscillations to converge to a steady state varies quite widely depending on the initializing sequence; in other words, the dynamical trajectories seem to be highly sensitive to initial conditions, again pointing to chaotic properties. Preliminary investigations indicated that the dynamical trajectory of the system was also highly sensitive to tiny perturbations to membrane potentials (at a single time instant) during the oscillatory phase, further supporting chaotic dynamics.

4 Discussion

Two spiking neural networks Net_A and Net_B , performing a simplified version of the memory span test, were analyzed. The memory span test was used simply as an example of a task that requires self-sustained activity in a non-trivial context, rather than to explicitly model memory. The focus of this explorations has been on neural dynamics in self-sustained activity.

The parameters of Net_A and Net_B were evolved to carry out the task using delay periods of 25 ms and 500 ms, respectively. It was shown that, in Net_A the output neurons are inhibited during the cue period, recover from the hyperpolarization during the delay period and

Table 5 Values of K for each input sequence (from S_1 to S_6) and for the membrane potential of neurons 3 (v_3), 4 (v_4) and 5 (v_5)

Seq.	v_3	v_4	v_5
S_1	0.98	0.96	0.98
S_2	0.97	0.97	0.95
S_3	0.94	0.97	0.97
S_4	0.99	0.98	0.98
S_5	0.97	0.98	0.97
S_6	0.97	0.94	0.97

fire action potentials in the correct order during the response period. In Net_B , the output neurons start firing during the cue period, maintain their activity during the delay period and generate the correct output in the response period.

Both networks exploit the capacity of the neuron to fire an action potential at the end of the inhibition period. In Net_A , the rebound spike is the mechanism used by the network to delay the action potential of the output neurons until the response period. During the delay period, the membrane potentials of the output neurons recovered from the inhibitory synapses. On the other hand, in Net_B the rebound spike is the mechanism to maintain the network activity during the longer delay period and, eventually, to generate the correct output in the response period.

We have seen that whether or not a neuron fires an action potential after a period of synaptic inhibition depends on a combination of values for synaptic weight (W), synaptic conductance (τ) and the postsynaptic neuron state (v and u). The closer the neuron is to its resting state (the stable point in the parameter space of v and u), the bigger the set of values for W and τ that make a neuron fire a rebound spike (shown in Fig. 10). On the other hand, soon after a spike, when a neuron starts recovering from an action potential, a rebound spike will occur only for a small set of high values of W and τ . When the analysis was carried out considering fixed values of W and τ (i.e., without synaptic plasticity), it was shown that there is a threshold for the parameter u below which a neuron fires rebound spikes (as shown by the surface in Fig. 12).

The parameter analysis contributed to understanding why a presynaptic inhibitory neuron should fire at

low frequencies in order to generate rebound spikes in a postsynaptic neuron. When a postsynaptic neuron spikes, its parameter u crosses the threshold. While u is above the threshold, inhibitory spikes in the presynaptic neuron will be lost (will not cause rebound spikes). In order to have a one-to-one relation between the number of inhibitory and rebound spikes, the presynaptic neuron should wait for the recovery period of u firing at low frequencies. Another reason why the frequency should be low is that a rebound spike occurs at the end of the inhibition process. If the presynaptic neuron fires at a high frequency, its spikes will not wait for the end of the inhibitory current and consequently will not have a corresponding rebound. In summary, the parameter analysis described the conditions under which a neural system can exploit the rebound spikes generated in inhibitory neural circuits as a mechanism to sustain the system activity after the stimulation has been removed.

The self-sustained mechanism introduced here can operate, in a larger system, with other mechanisms such as excitatory recurrent networks and short-term synaptic plasticity. While the rebound spikes could participate, for instance, sustaining the neural activity during the delay period of a trial of a memory task, persistent activity in recurrent network could participate during the preparation for the response period [58,70]. The rebound spikes could also play a role in non-consciousness working memory tasks where persistent activity is not present [67]. The investigation of how the post-inhibitory rebound could operate with other mechanisms requires the development of another computational model of a larger scale network with plastic connections.

The dynamics of the mechanism introduced here has some common properties with the mechanism underlying abnormal regimes of spike-wave discharges (SWDs) in the absence of epilepsy as proposed in [1,73]. Spontaneous initiation by short-term stimuli, synchronized oscillations maintained by the network coupling structure and spontaneous termination are important properties of abnormal regimes of SWDs [39,40]. Similarly, in our model, self-sustained oscillations are triggered by transient, short-term stimuli from neurons 1, 2 and 3 during the first 75 ms. Besides, the maintenance of the oscillations does not arise from the properties of individual neurons (such as in pacemaker cells), but also from the coupling structure of the network. Neurons 4, 5 and 6 are nonoscilla-

tory by themselves and do not have a parameter that changes their individual behavior, such as the birth of a limit cycle in Andronov–Hopf bifurcation. The self-sustained oscillations spontaneously terminate by discontinuation of maintenance mechanisms, that is, by breaking the circuit of rebound spikes. Whether the mechanism proposed here can generate pathological regimes of synchronicity, as observed in the SWDs, would have to be investigated with another computational model.

Note that the neural mechanism introduced was developed without any restriction on the type of behavior (e.g., periodic, quasiregular, chaotic) of the self-sustained activity. Our aim was to reproduce the phenomenon of self-sustained activity without explicitly modeling a specific instance of it, that is, without adjusting or adding parameters to the system in order to reproduce a particular behavior. A preliminary analysis of the system using the 0-1 Test suggested that the self-sustained regimes have a chaotic behavior and seem to exhibit transient chaos. However, further studies using a larger set of stimuli, other network coupling structures and other mathematical methods could be used for a deeper understanding of the system and will be the subject of further work. It should be possible to use more detailed, computationally expensive methodologies such as bifurcation analysis [61] and Lyapunov exponent with saltation matrices and Poincaré section [7,44,45]. It will also be important to investigate the presence of other types of dynamical behavior such as chimera states and heteroclinic trajectories [2,37,48,49].

We point out that, although it is common to see references in the literature to postsynaptic neural spikes following synaptic excitation, it is also biologically plausible to have an action potential following a period of synaptic inhibition. This phenomenon can be explained by different mechanisms that respond to voltage changes by opening sodium and potassium channels on different timescales [24]. Different neuron models that exhibit rebound spikes have been proposed by Izhikevich, namely rebound burst, inhibition-induced spiking and inhibition-induced bursting (see [28] for details).

All in all, based on a theoretical and minimalist model, we have suggested that post-inhibitory rebound spikes could participate in self-sustaining neural activity after the stimulus offset. For analyt-

ical tractability, the number of neurons of the network was kept to a minimum. Implementing a more detailed model (e.g., with more neurons and plastic connections) would produce more complicated dynamics and would not allow the type of analysis carried out here. However, future work will include investigations of this neural mechanism in larger networks to further establish its operating conditions. Results from our initial, more abstract, model may already suggest some interesting directions for neurophysiological experiments aimed at investigating whether or not the inhibitory mechanism discovered in our synthesized models can be found in real neural circuits.

Declarations

Conflicts of interest The authors declare that they have no conflict of interest.

Open Access This article is licensed under a Creative Commons Attribution 4.0 International License, which permits use, sharing, adaptation, distribution and reproduction in any medium or format, as long as you give appropriate credit to the original author(s) and the source, provide a link to the Creative Commons licence, and indicate if changes were made. The images or other third party material in this article are included in the article's Creative Commons licence, unless indicated otherwise in a credit line to the material. If material is not included in the article's Creative Commons licence and your intended use is not permitted by statutory regulation or exceeds the permitted use, you will need to obtain permission directly from the copyright holder. To view a copy of this licence, visit <http://creativecommons.org/licenses/by/4.0/>.

References

1. Abbasova, K., Chepurinov, S., Chepurnova, N., Van Luijckelaar, G.: The role of perioral afferentation in the occurrence of spike-wave discharges in the WAG/RIJ model of absence epilepsy. *Brain Res.* **1366**, 257–262 (2010)
2. Afraimovich, V.S., Rabinovich, M.I., Varona, P.: Heteroclinic contours in neural ensembles and the winnerless competition principle. *Int. J. Bifurc. Chaos* **14**(04), 1195–1208 (2004)
3. Alves, L.F., Araujo Junior, F.L., Santos, B.A., Gomes, R.M.: A Network of spiking neurons performing a relational categorization task. In: Barone, D., Teles, E., Brackmann, C. (eds) *Computational Neuroscience. LAWCON 2017. Communications in Computer and Information Science*, vol 720. Springer, Cham. (2017)
4. Ambroise, M., Levi, T., Joucla, S., Yvert, B., Saïghi, S.: Real-time biomimetic central pattern generators in an FPGA for hybrid experiments. *Front. Neurosci.* **7**, 215 (2013)

5. Appleby, P.A.: A model of chemotaxis and associative learning in *c. elegans*. *Biol. Cybern.* **106**(6–7), 373–387 (2012)
6. Barak, O., Tsodyks, M., Romo, R.: Neuronal population coding of parametric working memory. *J. Neurosci.* **30**(28), 9424–9430 (2010)
7. Bizzarri, F., Brambilla, A., Gajani, G.S.: Lyapunov exponents computation for hybrid neurons. *J. Comput. Neurosci.* **35**(2), 201–212 (2013)
8. Bojanek, K., Zhu, Y., MacLean, J.: Cyclic transitions between higher order motifs underlie sustained asynchronous spiking in sparse recurrent networks. *PLoS Comput. Biol.* **16**(9), (2020)
9. Borges, F., Protachevich, P., Pena, R., Lameu, E., Higa, G., Kihara, A., Matias, F., Antonopoulos, C., de Pasquale, R., Roque, A., et al.: Self-sustained activity of low firing rate in balanced networks. *Phys. A Stat. Mech. Appl.* **537**, 122671122671 (2020)
10. Bunge, S.A., Klingberg, T., Jacobsen, R.B., Gabrieli, J.D.: A resource model of the neural basis of executive working memory. *Proc. Natl. Acad. Sci.* **97**(7), 3573–3578 (2000)
11. Conway, A.R., Kane, M.J., Bunting, M.F., Hambrick, D.Z., Wilhelm, O., Engle, R.W.: Working memory span tasks: a methodological review and user’s guide. *Psychon. Bull. Rev.* **12**(5), 769–786 (2005)
12. Dickinson, P.S.: Neuromodulation in invertebrate nervous systems. In: Arbib M. A. (ed) *The handbook of brain theory and neural networks*, pp. 631–634. MIT Press (1998)
13. Drew, P.J., Abbott, L.: Extending the effects of spike-timing-dependent plasticity to behavioral timescales. *Proc. Natl. Acad. Sci.* **103**(23), 8876–8881 (2006)
14. Erickson, M.A., Maramara, L.A., Lisman, J.: A single brief burst induces glur1-dependent associative short-term potentiation: a potential mechanism for short-term memory. *J. Cognit. Neurosci.* **22**(11), 2530–2540 (2010)
15. Fiebig, F., Lansner, A.: A spiking working memory model based on Hebbian short-term potentiation. *J. Neurosci.* **37**(1), 83–96 (2017)
16. Fujisawa, S., Amarasingham, A., Harrison, M.T., Buzsáki, G.: Behavior-dependent short-term assembly dynamics in the medial prefrontal cortex. *Nat. Neurosci.* **11**(7), 823 (2008)
17. Gottwald, G.A., Melbourne, I.: A new test for chaos in deterministic systems. *Proc. R. Soc. Lond. Ser. A Math. Phys. Eng. Sci.* **460**(2042), 603–611 (2004)
18. Gottwald, G.A., Melbourne, I.: On the implementation of the 0–1 test for chaos. *SIAM J. Appl. Dyn. Syst.* **8**(1), 129–145 (2009)
19. Gottwald, G.A., Melbourne, I.: The 0-1 test for chaos: A review. In: Skokos, C., Gottwald, G., Laskar, J. (eds) *Chaos detection and predictability. Lecture Notes in Physics*, vol 915. Springer, Berlin, Heidelberg. (2016)
20. Harris-Warrick, R.M., Marder, E.: Modulation of neural networks for behavior. *Ann. Rev. Neurosci.* **14**(1), 39–57 (1991)
21. Harvey, I.: The microbial genetic algorithm. In: *European Conference on Artificial Life*, pp. 126–133. Springer (2009)
22. Hashemi, M., Valizadeh, A., Azizi, Y.: Effect of duration of synaptic activity on spike rate of a Hodgkin-Huxley neuron with delayed feedback. *Phys. Rev. E* **85**(2), (2012)
23. Hebb D.O.: *The organization of behavior: A neurophysiological approach*. New York: Wiley, (1949)
24. Hodgkin, A.L., Huxley, A.F.: A quantitative description of membrane current and its application to conduction and excitation in nerve. *J. Physiol.* **117**(4), 500–544 (1952)
25. Humpstone, H.: *The psychological clinic. Mem. Span Tests* **12**(5–9), 196 (1919)
26. Husbands, P., Moiola, R., Shim, Y., Philippides, A., Vargas, P., O’Shea, M.: *Evolutionary robotics and neuroscience*. In: Vargas, P., Di Paolo, E., Harvey, I. and Husbands, P. (eds), *The horizons of evolutionary robotics*, MIT Press, pp. 17–63 (2014)
27. Izhikevich, E.M.: Simple model of spiking neurons. *IEEE Trans. Neural Netw.* **14**(6), 1569–1572 (2003)
28. Izhikevich, E.M.: Which model to use for cortical spiking neurons? *IEEE Trans. Neural Netw.* **15**(5), 1063–1070 (2004)
29. Izhikevich, E.M., Edelman, G.M.: Large-scale model of mammalian thalamocortical systems. *Proc. Natl. Acad. Sci.* **105**(9), 3593–3598 (2008)
30. Izquierdo, E.J., Lockery, S.R.: Evolution and analysis of minimal neural circuits for Klinotaxis in *Caenorhabditis elegans*. *J. Neurosci.* **30**(39), 12908–12917 (2010)
31. Kim, Y.: Identification of dynamical states in stimulated Izhikevich neuron models by using a 0–1 test. *J. Korean Phys. Soc.* **57**(6), 1363–1368 (2010)
32. Korkmaz, N., Öztürk, İ., Kiliç, R.: Modeling, simulation, and implementation issues of CPGS for neuromorphic engineering applications. *Compu. Appl. Eng. Educ* **26**(4), 782–803 (2018)
33. Kriener, B., Enger, H., Tetzlaff, T., Plesser, H.E., Gewaltig, M.O., Einevoll, G.T.: Dynamics of self-sustained asynchronous-irregular activity in random networks of spiking neurons with strong synapses. *Front. Comput. Neurosci.* **8**, 136 (2014)
34. Kusters, J., Cortes, J., van Meerwijk, W., Ypey, D., Theuvsen, A., Gielen, C.: Hysteresis and bistability in a realistic cell model for calcium oscillations and action potential firing. *Phys. Rev. Lett.* **98**(9), (2007)
35. Leroy, F., Brann, D.H., Meira, T., Siegelbaum, S.A.: Input-timing-dependent plasticity in the hippocampal ca2 region and its potential role in social memory. *Neuron* **95**(5), 1089–1102 (2017)
36. Loewenstein, Y., Mahon, S., Chadderton, P., Kitamura, K., Sompolinsky, H., Yarom, Y., Häusser, M.: Bistability of cerebellar purkinje cells modulated by sensory stimulation. *Nat. Neurosci.* **8**(2), 202–211 (2005)
37. Majhi, S., Bera, B.K., Ghosh, D., Perc, M.: Chimera states in neuronal networks: a review. *Phys. Life Rev.* **28**, 100–121 (2019)
38. Marder, E., Abbott, L., Turrigiano, G.G., Liu, Z., Golowasch, J.: Memory from the dynamics of intrinsic membrane currents. *Proc. Natl. Acad. Sci.* **93**(24), 13481–13486 (1996)
39. Medvedeva, T., Sysoeva, M., Lüttjohann, A., van Luijtelea, G., Sysoev, I.: Dynamical mesoscale model of absence seizures in genetic models. *Plos One* **15**(9), (2020)
40. Medvedeva, T.M., Sysoeva, M.V., van Luijtelea, G., Sysoev, I.V.: Modeling spike-wave discharges by a complex network of neuronal oscillators. *Neural Netw.* **98**, 271–282 (2018)
41. Mi, Y., Katkov, M., Tsodyks, M.: Synaptic correlates of working memory capacity. *Neuron* **93**(2), 323–330 (2017)

42. Muioli, R.C., Vargas, P.A., Husbands, P.: Synchronisation effects on the behavioural performance and information dynamics of a simulated minimally cognitive robotic agent. *Biol. Cybern.* **106**(6–7), 407–427 (2012)
43. Mongillo, G., Barak, O., Tsodyks, M.: Synaptic theory of working memory. *Science* **319**(5869), 1543–1546 (2008)
44. Nobukawa, S., Nishimura, H., Yamanishi, T., Liu, J.Q.: Analysis of chaotic resonance in Izhikevich neuron model. *PLoS One* **10**(9), (2015)
45. Nobukawa, S., Nishimura, H., Yamanishi, T., Liu, J.Q.: Chaotic states induced by resetting process in Izhikevich neuron model. *J. Artif. Intell. Soft Comput. Res.* **5**(2), 109–119 (2015)
46. Osaka, M., Osaka, N., Kondo, H., Morishita, M., Fukuyama, H., Aso, T., Shibasaki, H.: The neural basis of individual differences in working memory capacity: an fMRI study. *NeuroImage* **18**(3), 789–797 (2003)
47. Osaka, N., Osaka, M., Kondo, H., Morishita, M., Fukuyama, H., Shibasaki, H.: The neural basis of executive function in working memory: an fMRI study based on individual differences. *Neuroimage* **21**(2), 623–631 (2004)
48. Rabinovich, M.I., Huerta, R., Varona, P., Afraimovich, V.S.: Transient cognitive dynamics, metastability, and decision making. *PLoS Comput. Biol.* **4**(5), (2008)
49. Rabinovich, M.I., Zaks, M.A., Varona, P.: Sequential dynamics of complex networks in mind: consciousness and creativity. *Phys. Rep.* (2020). <https://doi.org/10.1016/j.physrep.2020.08.003>
50. Ranhel, J.: Neural assembly computing. *Neural Netw. Learn. Syst.* **23**(6), 916–927 (2012)
51. Roth, A., van Rossum, M.C.: Modeling synapses. *Comput. Model. Methods Neurosci.* **6**, 139–160 (2009)
52. Sanchez-Vives, M.V., McCormick, D.A.: Cellular and network mechanisms of rhythmic recurrent activity in neocortex. *Nat. Neurosci.* **3**(10), 1027–1034 (2000)
53. Santos, B., Barandiaran, X., Husbands, P., Aguilera, M., Bedia, M.: Sensorimotor coordination and metastability in a situated HKB model. *Connect. Sci.* **24**(4), 143–161 (2012)
54. Shilnikov, A., Calabrese, R.L., Cymbalyuk, G.: Mechanism of bistability: tonic spiking and bursting in a neuron model. *Phys. Rev. E* **71**(5), (2005)
55. Shim, Y., Philippides, A., Staras, K., Husbands, P.: Unsupervised learning in an ensemble of spiking neural networks mediated by ITDP. *PLoS Comput. Biol.* **12**(10), (2016)
56. Shu, Y., Hasenstaub, A., McCormick, D.A.: Turning on and off recurrent balanced cortical activity. *Nature* **423**(6937), 288–293 (2003)
57. Soares, G.E., Borges, H.E., Gomes, R.M., Oliveira, G.M.: Emergence of neuronal groups on a self-organized spiking neurons network based on genetic algorithm. In: *Neural networks (SBRN), 2010 11th Brazilian symposium on*, pp. 43–48. IEEE (2010)
58. Stokes, M.G.: ‘activity-silent’ working memory in prefrontal cortex: a dynamic coding framework. *Trends Cognit. Sci.* **19**(7), 394–405 (2015)
59. Suvrathan, A.: Beyond STDP-towards diverse and functionally relevant plasticity rules. *Curr. Opin. Neurobiol.* **54**, 12–19 (2019)
60. Szatmáry, B., Izhikevich, E.M.: Spike-timing theory of working memory. *PLoS Comput. Biol.* **6**(8), (2010)
61. Tamura, A., Ueta, T., Tsuji, S.: Bifurcation analysis of Izhikevich neuron model. *Dyn. Contin. Discrete impuls. Syst. Ser. A Math. Anal.* **16**(6), 759–775 (2009)
62. Tél, T.: The joy of transient chaos. *Chaos Interdiscip. J. Non-linear Sci.* **25**(9), (2015)
63. Toker, D., Sommer, F.T., D’Esposito, M.: A simple method for detecting chaos in nature. *Commun. Biol.* **3**(1), 1–13 (2020)
64. Tolmachev, P., Dhingra, R.R., Pauley, M., Dutschmann, M., Manton, J.H.: Modeling the respiratory central pattern generator with resonate-and-fire izevich-neurons. In: *International conference on neural information processing*, pp. 603–615. Springer (2018)
65. Tomov, P., Pena, R.F., Roque, A.C., Zaks, M.A.: Mechanisms of self-sustained oscillatory states in hierarchical modular networks with mixtures of electrophysiological cell types. *Front. Comput. Neurosci.* **10**, 23 (2016)
66. Tomov, P., Pena, R.F., Zaks, M.A., Roque, A.C.: Sustained oscillations, irregular firing, and chaotic dynamics in hierarchical modular networks with mixtures of electrophysiological cell types. *Front. Comput. Neurosci.* **8**, 103 (2014)
67. Trübtschek, D., Marti, S., Ojeda, A., King, J.R., Mi, Y., Tsodyks, M., Dehaene, S.: A theory of working memory without consciousness or sustained activity. *Elife* **6**, (2017)
68. Vasu, M.C., Izquierdo, E.J.: Evolution and analysis of embodied spiking neural networks reveals task-specific clusters of effective networks. In: *Proceedings of the genetic and evolutionary computation conference*, pp. 75–82. ACM (2017)
69. Wang, X.J.: Synaptic reverberation underlying mnemonic persistent activity. *Trends Neurosci.* **24**(8), 455–463 (2001)
70. Watanabe, K., Funahashi, S.: Prefrontal delay-period activity reflects the decision process of a saccade direction during a free-choice odr task. *Cereb. Cortex* **17**(suppl–1), i88–i100 (2007)
71. Williams, S.R., Christensen, S.R., Stuart, G.J., Häusser, M.: Membrane potential bistability is controlled by the hyperpolarization-activated current IH in rat cerebellar purkinje neurons in vitro. *J. Physiol.* **539**(2), 469–483 (2002)
72. Womack, M., Khodakhah, K.: Active contribution of dendrites to the tonic and trimodal patterns of activity in cerebellar purkinje neurons. *J. Neurosci.* **22**(24), 10603–10612 (2002)
73. Zheng, T.W., O’Brien, T.J., Morris, M.J., Reid, C.A., Jovanovska, V., O’Brien, P., Van Raay, L., Gandrathi, A.K., Pinault, D.: Rhythmic neuronal activity in s2 somatosensory and insular cortices contribute to the initiation of absence-related spike-and-wave discharges. *Epilepsia* **53**(11), 1948–1958 (2012)

Publisher’s Note Springer Nature remains neutral with regard to jurisdictional claims in published maps and institutional affiliations.